SPECIAL TOPIC — Smart design of materials and design of smart materials

Stress effect on lattice thermal conductivity of anode material $NiNb_2O_6$ for lithium-ion batteries

Ao Chen(陈奥)[1], Hua Tong(童话)[1], Cheng-Wei Wu(吴成伟)[1], Guofeng Xie(谢国锋)[1], Zhong-Xiang Xie(谢忠祥)[2,†], Chang-Qing Xiang(向长青)[3,‡], and Wu-Xing Zhou(周五星)[1,§]

[1] *School of Materials Science and Engineering & Hunan Provincial Key Laboratory of Advanced Materials for New Energy Storage and Conversion, Hunan University of Science and Technology, Xiangtan* 411201, *China*

[2] *School of Science, Hunan Institute of Technology, Hengyang* 421002, *China*

[3] *College of Information Science and Engineering, Jishou University, Jishou* 416000, *China*

(Received 15 October 2022; revised manuscript received 6 December 2022; accepted manuscript online 9 December 2022)

The thermal transport properties of $NiNb_2O_6$ as anode material for lithium-ion battery and the effect of strain were studied by machine learning interatomic potential combined with Boltzmann transport equation. The results show that the lattice thermal conductivity of $NiNb_2O_6$ along the three crystal directions [100], [010], and [001] are 0.947 $W{\cdot}m^{-1}{\cdot}K^{-1}$, 0.727 $W{\cdot}m^{-1}{\cdot}K^{-1}$, and 0.465 $W{\cdot}m^{-1}{\cdot}K^{-1}$, respectively, indicating the anisotropy of the lattice thermal conductivity of $NiNb_2O_6$. This anisotropy of the lattice thermal conductivity stems from the significant difference of phonon group velocities in different crystal directions of $NiNb_2O_6$. When the tensile strain is applied along the [001] crystal direction, the lattice thermal conductivity in all three directions decreases. However, when the compressive strain is applied, the lattice thermal conductivity in the [100] and [010] crystal directions is increased, while the lattice thermal conductivity in the [001] crystal direction is abnormally reduced due to the significant inhibition of compressive strain on the group velocity. These indicate that the anisotropy of thermal conductivity of $NiNb_2O_6$ can be enhanced by the compressive strain, and reduced by the tensile strain.

Keywords: nickel niobate, lattice thermal conductivity, uniaxial strain, machine learning potential

PACS: 82.47.Aa, 74.25.fc, 44.10.+i, 66.70.–f **DOI:** 10.1088/1674-1056/acaa2d

1. Introduction

Lithium-ion batteries (LIBs) are widely applied in electrical vehicles and energy storage devices[1] because of their high voltage, high specific energy density, long cycle life, and wide working temperature range.[2] Meanwhile, the development of next-generation LIBs requires better performance in energy density, rapid recharge capability, safety, *etc*.[3] Therefore, numerous methods have been taken to improve the performance of pre-existing materials[4–7] or search for new high-performance materials during the past few years.[8,9] Recently, Xia *et al*.[10] reported that the nickel niobate ($NiNb_2O_6$), with a capacity of about 244 mAh/g^{-1} at low current densities, as cathode material for high-rate LIBs for the first time. The minimal volume change during lithiation gives rise to 81% capacity retention after 20000 cycles at 100 C. Besides, $NiNb_2O_6$ enables fast charging by virtue of a high diffusion coefficient of 10^{-12} $cm^2{\cdot}s^{-1}$ at 300 K.

Currently, researches on electrode materials mainly focus on increasing energy density, cycle efficiency, recharge capacity, safety, *etc*.[11–14] Myriad Joule heat generated by the current during the charging and discharging process. If the inherent heat transfer properties of LIBs are weak and the thermal dissipation efficiency is low, the cycle performance and the safety of the battery will be affected severely, even leading to thermal runaway of the battery.[15] In addition, quantity of accumulated heat leads to increasing temperature, which impinges the internal electrochemical reaction process of LIBs, resulting in sensitive performance and service life to temperature.[16] Despite the limited research scope of thermal transport properties of LIBs, a few studies have been carried out and some progress were achieved.[17–22] In 2019, He *et al*.[23] used molecular dynamics (MD) simulation to study the lattice thermal conductivity of lithium cobalt oxide ($LiCoO_2$), a common cathode material for LIBs, including monocrystalline and polycrystalline $LiCoO_2$. They found that monocrystalline $LiCoO_2$ exhibits a thermal conductivity of exceeding 100 $W{\cdot}m^{-1}{\cdot}K^{-1}$ with strong orientation dependence at room temperature, while the thermal conductivity of polycrystalline $LiCoO_2$ is isotropy and lower than 10 $W{\cdot}m^{-1}{\cdot}K^{-1}$. Meng *et al*.[24] explored the thermal conductivity of solid electrolyte polyethylene oxide (PEO) at room temperature. The results show that the thermal conductivity of crystalline PEO (60 $W{\cdot}m^{-1}{\cdot}K^{-1}$) is two orders of magnitude higher than that of amorphous PEO (0.37 $W{\cdot}m^{-1}{\cdot}K^{-1}$) at room temperature.

†Corresponding author. E-mail: xiezxhu@163.com

‡Corresponding author. E-mail: changqingxiang@jsu.edu.cn

§Corresponding author. E-mail: wuxingzhou@hnu.edu.cn

© 2023 Chinese Physical Society and IOP Publishing Ltd

Abdullaev *et al.*[25] studied the nanoscale thermal transport properties of lithiated amorphous silicon (a-Si) anode films experimentally. This study shows 40% increase in thermal conductivity of a-Si upon electrochemical lithiation reaching up to 2.2 $W{\cdot}m^{-1}{\cdot}K^{-1}$. In 2020, Yang *et al.*[26] studied the thermal conductivity of assorted cathode materials ($LiCoO_2$, $LiMnO_2$, $LiNiO_2$) at room temperature, which is 45.9 $W{\cdot}m^{-1}{\cdot}K^{-1}$, 6.0 $W{\cdot}m^{-1}{\cdot}K^{-1}$, and 8.9 $W{\cdot}m^{-1}{\cdot}K^{-1}$, respectively. Steinhardt *et al.*[27] investigated the thermal conductivity of nickel manganese cobalt (NMC) cathode and graphite anode materials with respect to battery states, such as temperature and in-plane pressure, through experiments. According to the measurement result, the thermal conductivity increases by 11.9% when the pressure rises by 37.1 kPa, and simultaneously decreases by more than 1% when the temperature increases by 1 K compared to the absolute value at 20 K. In addition, Wu *et al.*[28,29] analyzed and discussed the heat transfer performance and thermal stability of solid electrolyte. Jiang *et al.*[16] and Toledo Quiroz *et al.*[30] studied the thermal management of LIBs at high temperatures and proposed cooling methods.

In view of the excellent performance of $NiNb_2O_6$, it is of great significance to understand the thermal transport performance in order to achieve application, yet no corresponding researches have been reported hitherto. In this work, these properties are systematically studied via machine learning interatomic interaction potential (MLIP)[31,32] combined with ShengBTE package.[33] Moreover, the MLTP is developed from the training database, which is generated from the trajectory through *ab initio* molecular dynamics (AIMD) method.[31] in Vienna *ab initio* simulation package (VASP).[34] Additionally, the generation of strain (ε) is inexorable during the charging and discharging process of LIBs,[35] *e.g.*, the nanostrain accumulated in Li- and Mn-rich (LMR) cathode materials.[36] Therefore, we also studied the influence of the uniaxial stress (strain range is from $\varepsilon = -4\%$ to $\varepsilon = 4\%$) along the [001] crystal direction to thermal transport properties. Moreover, the results of calculating the phonon dispersion relation for different strains show that the Ni_2NbO_6 structure can remains stable under 4% tensile or compressive strain.

2. Models and methods

$NiNb_2O_6$ has an orthorhombic crystal structure with a space group of *Pbcn*,[37] which is diagramed in Figs. 1(a) and 1(b). There are 8 Nb atoms, 4 Ni atoms, and 24 O atoms in each primitive unit cell, both of the Ni^{2+} and Nb^{5+} ions exhibit a coordination number of 6, forming octahedrons with surrounding O atoms. All of NiO octahedron layers are composed of corner-shared NiO octahedrons, detached by two intercalated NbO octahedron layers. Wherein, the unit cell vectors of a, b, and c are parallel to [100], [010], and [001] crystal orientation, respectively.

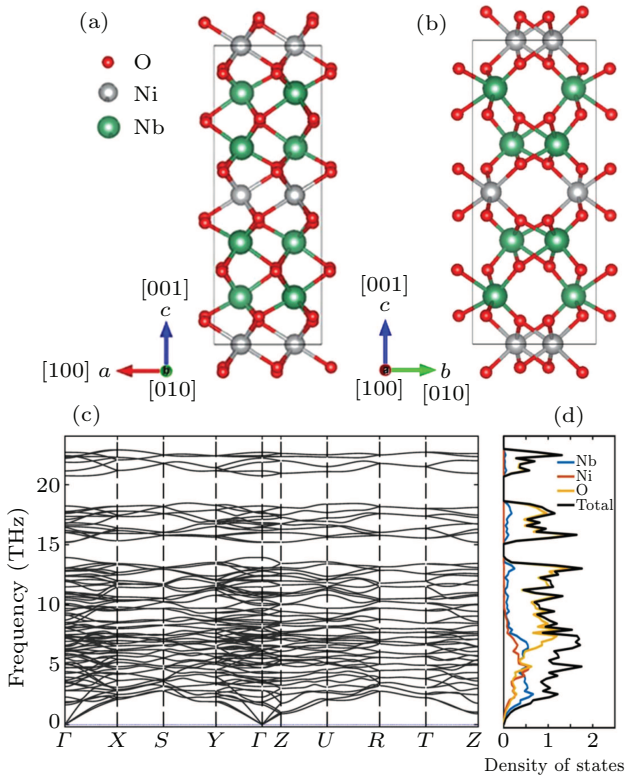


Fig. 1. (a) and (b) Schematic diagrams of primitive cell, (c) the phonon dispersion, (d) projected density of states of $NiNb_2O_6$.

Our calculations are based on the phonon Boltzmann transport equation (PBTE) method, which gives the lattice thermal conductivity (κ_p) by

$$\kappa_p^{\alpha\beta} = \frac{1}{N\Omega k_B T^2} \sum_{\lambda} f_0(f_0+1)(\hbar\omega_\lambda)^2 v_\lambda^\alpha v_\lambda^\beta \tau_\lambda, \qquad (1)$$

where α, β are the coordinate direction, N is the phonon wave vector number, Ω is the volume of each primitive unit cell, k_B is the Boltzmann constant, T is the absolute temperature, f_0 is the Bose–Einstein distribution function, $\hbar$ is the reduced Planck constant. ω_λ and τ_λ is the phonon angular frequency and relaxation time of vibration mode of branch λ, respectively, v_λ^α is phonon group velocity of vibration mode of branch λ along α coordinate direction.

According to Eq. (1), the key step to calculate the κ_p of $NiNb_2O_6$ is to obtain v_λ and τ_λ. We can attain the harmonic properties, such as phonon dispersion relation and group velocity, and anharmonic properties such as phonon relaxation time[38] via the second-order interatomic force constants (2nd IFCs) and the third-order IFCs (3rd IFCs), which are commonly obtained from the first-principle calculations based on the density functional theory (DFT)[39] or MD simulation.[20] DFT calculations are quite precise, whereas the application scale is limited with huge cost when applied to multi-atomic systems. In spite of extended application scale of MD simulation, the accuracy of utilizing empirical potential cannot be

guaranteed, with plentiful systems lacking appropriate empirical potential. During past few years, MLIPs have provided another promising method to calculate the 2nd IFCs and 3rd IFCs,[31,32] which has been implemented to model the structure, investigate thermodynamic and mechanical properties of partial materials,[40–42] the properties of grain boundaries of polycrystalline Si,[43] the thermal conductivity of crystalline Si and a-Si,[44] $NiNb_2O_6$ is a promising electrode material lacking empirical potential, which is of importance in calculating thermal properties and mechanical properties. Hence, we developed corresponding MLIP via machine learning method to study the properties of $NiNb_2O_6$.

All of the first-principle calculations are implemented with DFT via VASP, the projector authenticated wave (PAW) pseudopotential is applied to portray the interaction among atoms.[45] The generalized gradient approximation (GGA) with the Perdew–Bourke–Ernzerhof (PBE) exchange–correlation function is adopted for structure relaxation.[46] The kinetic energy cut-off of the plane-wave basis is set to 520 eV, which is converged after testing. A Monkhorst–Pack *k*-mesh of $3 \times 3 \times 1$ is employed to sample the Brillouin zones of the primitive unit cell. The structure optimization is carried out until the atom positions and lattice constants are completely relaxed, when the forces on each atom are less than 10^{-4} eV·Å^{-1} and the energy of system is converged at 10^{-6} eV. The results of first-principle calculation show that the relaxed lattice parameter of $NiNb_2O_6$ is 5.075 Å, 5.763 Å, and 14.169 Å for *a*, *b*, and *c* unit cell vectors respectively, which is consistent with the experimental data of 5.015 Å, 5.675 Å, and 14.022 Å.[10] A $3 \times 3 \times 3$ supercell is adopted during the AIMD simulation at 50 K, the simulation lasts for 400 fs with the time step of 1 fs. Then the MLIP is developed from the training database composed of the trajectory of atoms. A supercell of $3 \times 3 \times 3$ is employed when the 2nd IFCs and 3rd IFCs are calculated with the MLIP, respectively. Based on the 2nd IFCs calculated by MLIP, the phonon dispersion curve can be obtained by the Phonopy[47] code is depicted in Fig. 1(c), where no imaginary frequency appears in the phonon dispersion curve, which illustrates the dynamic stability of $NiNb_2O_6$. Besides, the projected density of states (DOS) indicates that the Ni and Nb atoms contribute a lot acoustic to the phonon branches and low-frequency optical phonon branches below 8 THz while the O atoms mainly contribute to high-frequency optical phonons. The κ_p derives from solving the PBTE iteratively, and a dense phonon q-grid of $12 \times 12 \times 6$ is implemented to achieve convergence.

In this paper, the stress is employed by setting the strain, which means changing the lattice constant. Moreover, the uniaxial stress applied along the [001] lattice direction has been restricted, corresponding to the strain range between -4% to 4%, due to the existence of imaginary frequency, with the lattice structure and space group remaining unchanged when stress applied.

3. Results and discussion

We firstly study the thermal transport properties of $NiNb_2O_6$ under free state, which is manifested as the dependence of κ_p to temperature from 200 K to 800 K. In Fig. 2(a), the tendency of κ_p along [100], [010], and [001] crystal orientations ($\kappa_{[100]}$, $\kappa_{[010]}$, $\kappa_{[001]}$) are given respectively, from where we can see that the κ_p decreases inversely with temperature, which is due to the increasing scattering intensity of phonons with elevated temperature, leading to the free path of phonons presenting a inversely proportion to temperature. Also, the κ_p of $NiNb_2O_6$ exhibits a remarkable anisotropy at room temperature, $\kappa_{[100]}$, $\kappa_{[010]}$, and $\kappa_{[001]}$ are 0.947 W·m^{-1}·K^{-1}, 0.727 W·m^{-1}·K^{-1}, and 0.465 W·m^{-1}·K^{-1}, respectively. Wherein, $\kappa_{[100]}$ and $\kappa_{[010]}$ are twice and 1.5 times the value of $\kappa_{[001]}$. To reveal the cause of the remarkable anisotropy, the distribution of group velocity along three crystal orientation with respect to frequency under free state is illustrated intuitionally in Fig. 2(b). The figure indicates that the anisotropy of group velocity is remarkable when frequency is lower than 13 THz, *e.g.*, the group velocity along [100] crystal orientation is obviously larger than that along [001] crystal orientation, which interprets the anisotropy of κ_p appropriately. Actually, the discrepancy of high-frequency group velocity is not comparable to low-frequency group velocity because the acoustic phonons and low-frequency phonons contributes dominantly to κ_p generally.

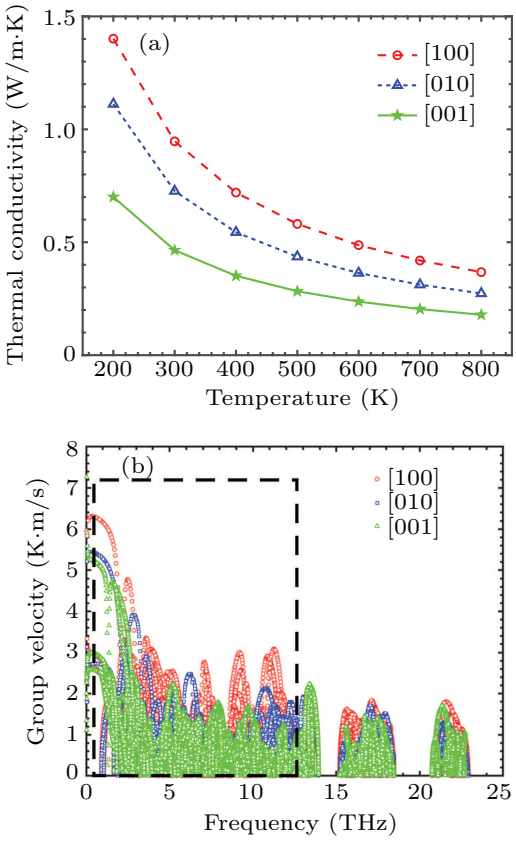


Fig. 2. (a) Thermal conductivity *versus* temperature and (b) group velocity *versus* frequency without stress at 300 K.

Except for the thermal transport properties of materials, the κ_p of the battery is associated with a variety of factors, *e.g.*, Li-ion concentration, accumulative stress, crystallinity, *etc*. In particular, a large amount of strain will accumulate as the charging and discharging reaction proceeds,[48] which has been proved of dominant influence to the thermal transport performance recently. Feng *et al.*[49] further explored the influence of uniaxial stress applied along the z axis on the thermal conductivity of delithiated $Li_{0.33}CoO_2$. The results demonstrates that 2% tensile strain can reduce the thermal conductivity to almost zero while 2% compressive strain can increase the in-plane thermal conductivity and through-plane thermal conductivity by 30% and 80%, respectively. Actually, the calculation found that $NiNb_2O_6$ is a sort of material with normal poisson's ratio (~ 0.3), which indicates that stretch or compress in one direction, and compression or tensile strain will occur in other directions, as shown in Table 1. Therefore, the strain dependence of lattice thermal conductivity in different directions can be obtained simultaneously by stretching or compressing along a certain direction.

Table 1. Lattice parameters along three crystal directions under various strains.

Strain (%)	Lattice parameters (Å)		
	[100]	[010]	[001]
–4	5.137	5.853	13.602
–2	5.106	5.808	13.885
0	5.075	5.763	14.169
2	5.044	5.721	14.452
4	5.015	5.680	14.735

In this work, uniaxial stress along [001] crystal direction is applied to explore the effect of stress on the thermal transport properties of $NiNb_2O_6$, then the thermal conductivity of $NiNb_2O_6$ under different stress states at room temperature is calculated. Multiple research results demonstrate that the thermal conductivity of solid-state materials will increase under compressive stress,[49–53] whereas decrease under tensile stress.[49,50,53,54] However, there are several researches indicating different trends.[20,55–57] Figure 3 displays the tendency of κ_p of $NiNb_2O_6$ under different strain states at room temperature. It is notable that the tendency of κ_p along different crystal orientation varies considerably. Compared with the free state, $\kappa_{[100]}$ and $\kappa_{[010]}$ increase by 12% and 16% under -4% compressive strain state and decrease by 29% and 20% under 4% tensile strain state, respectively. It is obvious that $\kappa_{[100]}$ and $\kappa_{[010]}$ decrease with the compressive strain converted to tensile strain. Nevertheless, $\kappa_{[001]}$ presents an opposite tendency that decreasing under both of the tensile and compressive strain, which are reduced by 17% and 32% under 4% tensile strain and -4% compressive strain. Meanwhile, we note that the implementation of strain does not convert the anisotropy of κ_p, but compressive strain strengthens the anisotropy while the tensile strain plays the opposite role. The discrepancy of response of κ_p to strain along different crystal orientations could be elaborated by the multiple responses to strain of phonon transport properties.

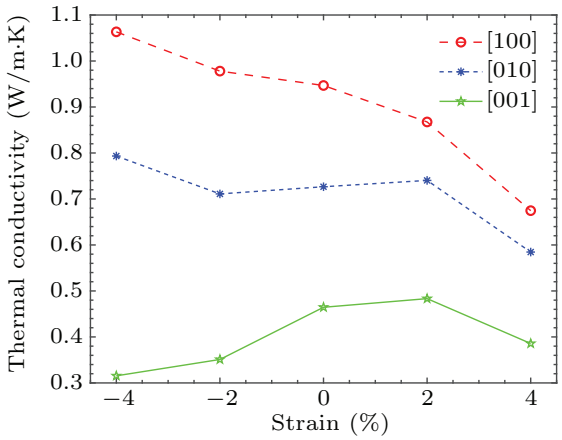


Fig. 3. Thermal conductivity of $NiNb_2O_6$ under distinct strain states at 300 K.

Furthermore, we display the normalized cumulative κ_p of $NiNb_2O_6$ along three different crystal orientations with respect to frequency under three strain states at 300 K, as depicted in Fig. 4, to clarify the contribution of phonons to the κ_p at different frequency ranges. It can be seen that the contribution to κ_p reaches 80% under 10 THz in most conditions, *e.g.*, the proportion exceeds 90% under -4% strain state, as shown in Fig. 4(b), suggesting that the main contribution to the κ_p still stems from the acoustic phonons and low-frequency optical phonons ($\omega < 10$ THz) under different strain states. Therefore, the subsequent analysis is mainly concentrated on phonon properties with frequencies below 10 THz.

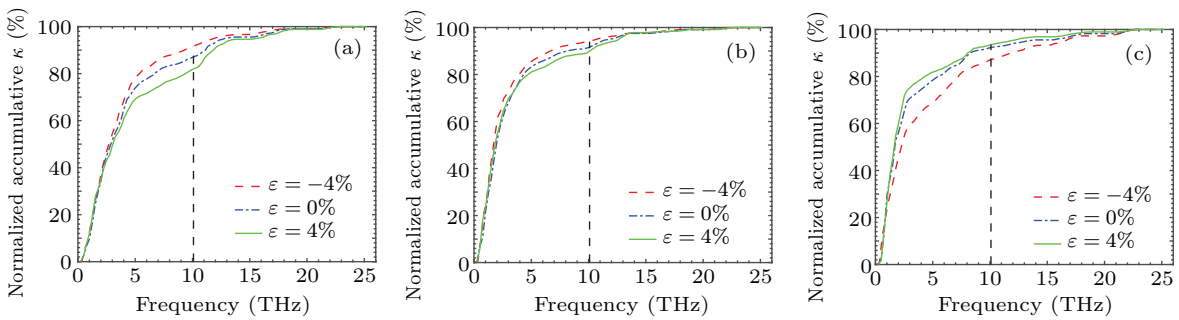


Fig. 4. Normalized accumulative thermal conductivity as a function of frequency at 300 K along (a) [100] lattice direction, (b) [010] lattice direction, and (c) [001] lattice direction under three strain states ($\varepsilon = -4\%$, $\varepsilon = 0\%$, $\varepsilon = 4\%$).

In order to explore the underlying strain-influence on different properties of phonons, we give the phonon scattering rate of $NiNb_2O_6$ under different strain states at room temperature in Fig. 5. The higher the scattering rate is, the larger the κ_p becomes, which is because relaxation time is the reciprocal of scattering rate. The results suggest that, compared with the free state, the scattering rate slightly rises under no matter compressive or tensile strain, which stems from the weakened bonding strength that enhances the anharmonicity of the system because of strain.[58] However, the tiny change of the scattering rate cannot convincingly interpret the remarkable variety of κ_p, which promotes further analysis on the effect of group velocity on the κ_p.

In Fig. 6, the distributions of the phonon group velocity *versus* frequency along [100], [010], and [001] crystal orientations are displayed, where the ranges below 5 THz with significant changes are highlighted. As shown in Figs. 6(a) and 6(b), the group velocity along the [100] and [010] crystal directions under the compressive strain increases significantly, compared with free state, while correspondingly decreasing under the tensile strain, which presents the similar tendency to κ_p. Nonetheless, figure 6(c) indicates that both of the phonon group velocity along the [001] crystal direction under strain state are lower than that under free state, which corresponds to the tendency of κ_p (reduced by 32% and 17% under −4% and 4% strain states). Herein, the phonon group velocity takes the dominant contribution to κ_p while tuning through strain.

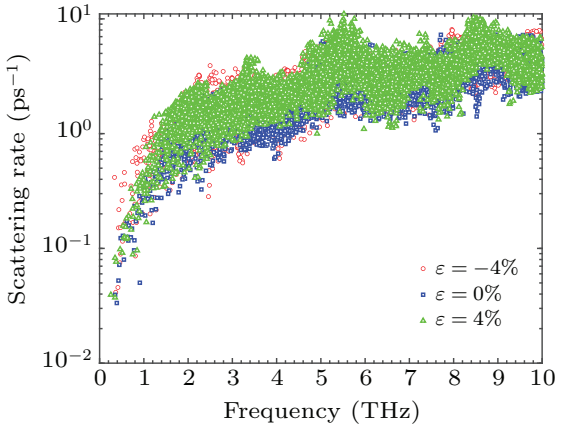


Fig. 5. The phonon scattering rate under three strain states at 300 K.

Additionally, given that electrodes in realistic LIBs are usually made of polycrystalline, whose thermal conductivity ought to be different from that of monocrystalline. Moreover, based on some empirical formulas,[59] the thermal conductivity of polycrystalline $NiNb_2O_6$ can be calculated from the intrinsic thermal conductivity of monocrystalline $NiNb_2O_6$. Therefore, the monocrystalline thermal conductivity in this work could provide information for researches on polycrystalline thermal conductivity which could be obtained by the empirical equation.

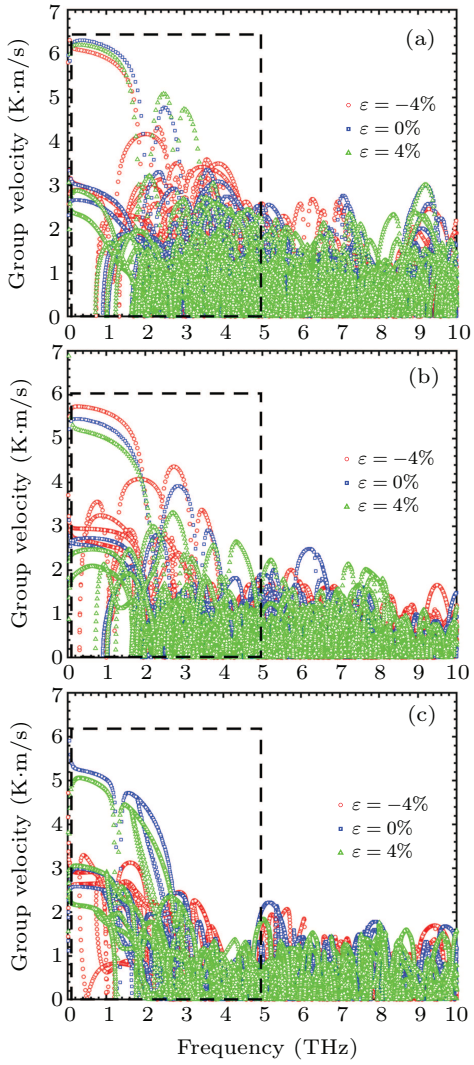


Fig. 6. Group velocity along (a) [100] lattice direction, (b) [010] lattice direction, and (c) [001] lattice direction under three strain states at 300 K.

4. Conclusions

Using the MLIP combined with Boltzmann transport equation, the lattice thermal conductivity of $NiNb_2O_6$ and the effect of strain were investigated. The κ_p of $NiNb_2O_6$ exhibits a remarkable anisotropy ($\kappa_{[100]}$, $\kappa_{[010]}$, and $\kappa_{[001]}$ is 0.947 W·m^{-1}·K^{-1}, 0.727 W·m^{-1}·K^{-1}, and 0.465 W·m^{-1}·K^{-1}, respectively), which is attributed to the anisotropy of the phonon group velocity. Additionally, the effect of strain on κ_p presents great discrepancy, *e.g.*, −4% compressive strain could improve the $\kappa_{[100]}$ and $\kappa_{[010]}$ by around 12% and 16% while 4% tensile strain reduces the $\kappa_{[100]}$ and $\kappa_{[010]}$ by around 29% and 30%, respectively. However, the existence of strain is disadvantageous to the thermal transport along [001] crystal direction, no matter compression or tension, where −4% compressive strain and 4% tensile strain reduce the $\kappa_{[001]}$ by around 32% and 17%, respectively. Furthermore, the implementation of compressive strain will strengthen the anisotropy with the tensile strain exhibiting the opposite phenomenon. By analyzing the tendency of phonon

properties with respect to strain, the regulation of strain on κ_p is ascribed to the effect on phonon group velocity, which may deepen the understanding of the thermal transport properties of $NiNb_2O_6$ as anode material for LIBs and reveal the underlying mechanism of strain tuning thermal transport.

Acknowledgements

Project supported by the National Natural Science Foundation of China (Grant Nos. 12074115 and 11874145) and the Natural Science Foundation of Hunan Province, China (Grant No. 2021JJ30202).

References

[1] Tarascon J M and Armand M 2001 *Nature* **414** 359
[2] Yue J L, Zhou Y N, Shi S Q, Shadike Z, Huang X Q, Luo J, Yang Z Z, Li H, Gu L, Yang X Q and Fu Z W 2015 *Sci. Rep.* **5** 8810
[3] Goodenough J B and Kim Y 2010 *Chem. Mater.* **22** 587
[4] Du A, Li H, Chen X, Han Y, Zhu Z and Chu C 2022 *ChemistrySelect* **7** e202201269
[5] Eftekhari A 2017 *J. Power Sources* **343** 395
[6] Yang F, Feng X, Glans P A and Guo J 2021 *APL Materials* **9** 050903
[7] Wang Y Q, Sun X R, Xiao R H and Chen L Q 2020 *Chin. Phys. B* **29** 038202
[8] Venugopal B, Syum Z, Yu S Y, sabbah A, Shown I, Chu C W, Chen L C, Lee C H, Wu H L and Chen K H 2022 *ACS Omega* **7** 9152
[9] Zhao Q, Peng P, Zhu P, Yang G, Sun X, Ding R, Gao P and Liu E 2022 *New J. Chem.* **46** 9612
[10] Xia R, Zhao K, Kuo L Y, Zhang L, Cunha D M, Wang Y, Huang S, Zheng J, Boukamp B, Kaghazchi P, Sun C, ten Elshof J E and Huijben M 2021 *Adv. Energy Mater.* **12** 2102972
[11] Soavi F, Brilloni A, De Giorgio F and Poli F 2022 *Current Opinion in Chemical Engineering* **37** 100835
[12] Li S, Shi X Y, Tang Z P, Li D X, Zhang Y C, Xiao Y, Song Y, Zheng Z, Zhong Y J, Wu Z G, Zhong B H and Guo X D 2022 *Appl. Surf. Sci.* **585** 152643
[13] Weiss M, Ruess R, Kasnatscheew J, Levartovsky Y, Levy N R, Minnmann P, Stolz L, Waldmann T, Wohlfahrt-Mehrens M, Aurbach D, Winter M, Ein-Eli Y and Janek J 2021 *Adv. Energy Mater.* **11** 2101126
[14] Liu K, Liu Y, Lin D, Pei A and Cui Y 2018 *Sci. Adv.* **4** eaas9820
[15] Xiang C, Wu C W, Zhou W X, Xie G and Zhang G 2021 *Front. Phys.* **17** 13202
[16] Jiang Z Y, Li H B, Qu Z G and Zhang J F 2022 *Int. J. Hydrogen Energy* **47** 9428
[17] Wu C W, Ren X, Zhou W X and Xie G 2022 *Acta Phys. Sin.* **71** 027803 (in Chinese)
[18] Suwardi A, Cao J, Hu L, *et al.* 2020 *J. Mater. Chem. A* **8** 18880
[19] Suwardi A, Cao J, Zhao Y, Wu J, Chien S W, Tan X Y, Hu L, Wang X, Wang W, Li D, Yin Y, Zhou W X, Repaka D V M, Chen J, Zheng Y, Yan Q, Zhang G and Xu J 2020 *Mater. Today Phys.* **14** 100239
[20] Chen X K, Hu X Y, Jia P, Xie Z X and Liu J 2021 *Int. J. Mech. Sci.* **206** 106576
[21] Zhou W X, Cheng Y, Chen K Q, Xie G, Wang T and Zhang G 2020 *Adv. Funct. Mater.* **30** 1903829
[22] Jia P Z, Zeng Y J, Wu D, Pan H, Cao X H, Zhou W X, Xie Z X, Zhang J X and Chen K Q 2019 *J. Phys.: Condens. Matter* **32** 055302
[23] He J, Zhang L and Liu L 2019 *Phys. Chem. Chem. Phys.* **21** 12192
[24] Meng H, Yu X, Feng H, Xue Z and Yang N 2019 *Int. J. Heat Mass Transfer* **137** 1241
[25] Abdullaev A, Mukanova A, Yakupov T, Mentbayeva A, Bakenov Z and Utegulov Z 2020 *Mater. Today Proc.* **25** 88
[26] Yang H, Savory C N, Morgan B J, Scanlon D O, Skelton J M and Walsh A 2020 *Chem. Mater.* **32** 7542
[27] Steinhardt M, Gillich E I, Stiegler M and Jossen A 2020 *J. Energy Storage* **32** 101680
[28] Wu C W, Ren X, Zhou W X, Xie G and Zhang G 2022 *APL Materials* **10** 040902
[29] Wu C W, Xie G F and Zhou W X 2022 *Acta Phys. Sin.* **71** 026501 (in Chinese)
[30] Toledo-Quiroz R A, Calderón-Muñoz W R and Paccha-Herrera E 2021 *J. Energy Storage* **44** 103394
[31] Mortazavi B, Podryabinkin E V, Novikov I S, Rabczuk T, Zhuang X and Shapeev A V 2021 *Comput. Phys. Commun.* **258** 107583
[32] Mortazavi B, Novikov I S, Podryabinkin E V, Roche S, Rabczuk T, Shapeev A V and Zhuang X 2020 *Appl. Mater. Today* **20** 100685
[33] Li W, Carrete J, A. Katcho N and Mingo N 2014 *Comput. Phys. Commun.* **185** 1747
[34] Kresse G and Furthmüller J 1996 *Phys. Rev. B* **54** 11169
[35] Balke N, Jesse S, Morozovska A N, Eliseev E, Chung D W, Kim Y, Adamczyk L, GarcíPa R E, Dudney N and Kalinin S V 2010 *Nat. Nanotechnol.* **5** 749
[36] Liu T, Liu J, Li L, *et al.* 2022 *Nature* **606** 305
[37] Yaeger I, Morrish A H and Wanklyn B M 1977 *Phys. Rev. B* **15** 1465
[38] Togo A and Tanaka I 2015 *Scr. Mater.* **108** 1
[39] Zhou W X and Chen K Q 2015 *Sci. Rep.* **5** 15070
[40] Bartók A P, Payne M C, Kondor R and Csányi G 2010 *Phys. Rev. Lett.* **104** 136403
[41] Behler J and Parrinello M 2007 *Phys. Rev. Lett.* **98** 146401
[42] Thiemann F L, Rowe P, Müller E A and Michaelides A 2020 *J. Phys. Chem. C* **124** 22278
[43] Fujii S and Seko A 2022 *Comp. Mater. Sci.* **204** 111137
[44] Qian X, Peng S, Li X, Wei Y and Yang R 2019 *Mater. Today Phys.* **10** 100140
[45] Blöchl P E 1994 *Phys. Rev. B* **50** 17953
[46] Perdew J P, Burke K and Ernzerhof M 1996 *Phys. Rev. Lett.* **77** 3865
[47] Togo A and Tanaka I 2015 *Scr. Mater.* **108** 1–5
[48] Wang H, Jang Y I, Huang B, Sadoway D R and Chiang Y M 1999 *J. Electrochem. Soc.* **146** 473
[49] Feng T, O'Hara A and Pantelides S T 2020 *Nano Energy* **75** 104916
[50] Chernatynskiy A and Phillpot S R 2013 *J. Appl. Phys.* **114** 064902
[51] Broido D A, Lindsay L and Ward A 2012 *Phys. Rev. B* **86** 115203
[52] Mukhopadhyay S and Stewart D A 2014 *Phys. Rev. Lett.* **113** 025901
[53] Tang D S, Qin G Z, Hu M and Cao B Y 2020 *J. Appl. Phys.* **127** 035102
[54] Parrish K D, Jain A, Larkin J M, Saidi W A and McGaughey A J H 2014 *Phys. Rev. B* **90** 235201
[55] Ouyang T and Hu M 2015 *Phys. Rev. B* **92** 235204
[56] Zhang P, Ouyang T, Tang C, He C, Li J, Zhang C and Zhong J 2020 *Physica E: Low-dimensional Systems and Nanostructures* **118** 113870
[57] Lindsay L, Broido D A, Carrete J, Mingo N and Reinecke T L 2015 *Phys. Rev. B* **91** 121202
[58] Zhang C, Sun J, Shen Y, Kang W and Wang Q 2022 *J. Phys. Chem. Lett.* **13** 5734
[59] Dong H, Wen B and Melnik R 2014 *Sci. Rep.* **4** 7037